In those parts of curves 4 in Figs. 1A and 2A in which Rb < Rb* it would appear that there is a transient distribution of t and u with respect to the coordinates; this exerts a major influence on the values of the coefficients K_q and K_m.

Thus the local Rb number may be regarded as a quantity characterizing the kinetic characteristics of the local drying of an elementary layer in the solid material and also the transfer properties of the latter.

NOTATION

Rb, Rb*, integral and local Rebinder numbers, respectively; u, $\bar{u}$, local and volume-average moisture contents; t, $\bar{t}$, local and volume-average temperatures; t_{am}, ambient (air) temperature; $j_m(\tau)$, $j_m^*(\tau)$, integrated and local moisture flow densities; $j_q(\tau)$, $j_q^*(\tau)$, integrated and local heat flow densities; r, specific heat of vaporization; ε, phase transformation number; a_q, a_m, heat and moisture diffusion coefficients; c_q, specific heat of moist material; γ_0, density of dry material; α_q, α_m, heat- and mass-transfer coefficients; δ, thermal-gradient mass-transfer coefficient; u_{eq}, equilibrium moisture content of the material; Pn, Posnov number; λ_q, λ_m, thermal and mass conductivities of the material; x, coordinate reckoned from the center of the plate; τ, time from the onset of drying. Indices: s, surface of the solid material as a whole or that of the elementary volume; cen, center of the solid.

LITERATURE CITED

1. A. V. Lykov, Theory of Drying [in Russian], Énergiya, Moscow (1968).
2. L. Ya. Volosyan, in: Heat and Mass Transfer during the Heat Treatment of Concrete and Reinforced Concrete Objects [in Russian], Nauka i Tekhnika, Minsk (1973).
3. V. P. Zhuravleva, in: Mass Transfer during the Heat Treatment and Drying of Capillary-Porous Building Materials [in Russian], Nauka i Tekhnika, Minsk (1972).
4. P. S. Kuts and A. I. Ol'shanskii, Inzh.-Fiz. Zh., 23, No. 6 (1972).
5. V. M. Kazanskii, Inzh.-Fiz. Zh., 26, No. 1 (1974).
6. M. F. Kazanskii and P. P. Lutsik, Inzh.-Fiz. Zh., 3, No. 11 (1960).
7. F. M. Polonskaya, Zh. Tekh. Fiz., 23, No. 5 (1953).
8. P. D. Lebedev, Infrared Drying [in Russian], GÉI, Moscow (1955).
9. A. S. Shubin, Radioisotope Study of Convective Drying Processes [in Russian], Moscow (1957).
10. P. P. Lutsik, in: Thermal Conductivity and Diffusion [in Russian], No. 5, Riga (1974).
11. M. F. Kazanskii, Dokl. Akad. Nauk SSSR, 130, No. 5 (1960).

MASS-TRANSFER AND STRUCTURAL-MECHANICS CHARACTERISTICS OF PLASTER OF PARIS

V. G. Kamenskii, G. S. Raptunovich, I. M. Lyashkevich, E. A. Raskina, L. G. Chernaya, and L. V. Krasulina

UDC 66.047

Results are presented on the thermodynamic parameters, mass transfer, porous structure, and state characteristics of plaster of paris.

In recent years, there has been extensive research for new and efficient means of producing modified types of artificial stone on the basis of materials such as plaster of paris, whose parameters are affected by various external factors (temperature, pressure, vibration, magnetic fields, etc.).

A. V. Lykov Institute of Heat and Mass Transfer, Academy of Sciences of the Belorussian SSR, Minsk.

Translated from Inzhenerno-Fizicheskii Zhurnal, Vol. 31, No. 1, pp. 54-59, July, 1976. Original article submitted June 12, 1975.

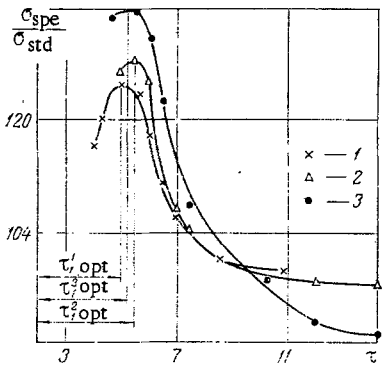

Fig. 1

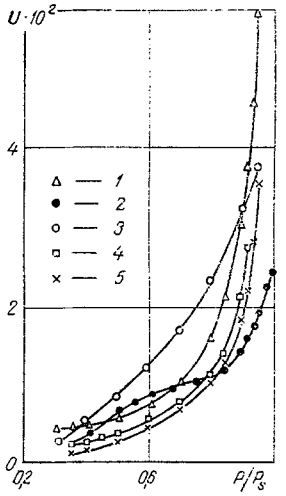

Fig. 2

Fig. 1. Relative increase $\sigma_{spe}/\sigma_{std}$ (%) in strength as a function of time: 1) steady magnetic field H = 226,900 A/m; 2) field at 50 Hz, 7960 A/m; 3) field at 30 Hz, 796 A/m.

Fig. 2. Isotherms for uptake of water vapor U (kg/kg) for gypsum as a function of P/P_S: 1) standard hardening; 2, 3) special treatment; 4) processed in a magnetic field with optimum parameters; 5) treated in a magnetic field.

This institute has previously carried out researches on the dissolution, nucleation, and crystal growth of gypsum [1,2], which has shown that a magnetic field has an appreciable effect on the kinetics of such processes, especially nucleation in the formation of gypsum from supersaturated aqueous solutions, since it increases the number of such nuclei per unit volume very considerably, while reducing the linear dimensions.

We have examined the physicomechanical, structural, and mass-transfer characteristics of cast plaster of paris made in the presence of magnetic fields and in response to various external factors.

We used plaster of paris as employed in building, which had the following parameters: normal consistency K_{nc} = 0.6, onset of setting 7'20", end of setting 14'8", and strength in compression σ_{co} = 65 kgf/cm^2.

The strength was examined by pouring a specimen 2 min after mixing into PTFE molds; after 1.5 h, the specimen was released from the mold and placed in a drying cabinet for drying at 55°C to constant weight, after which the strength was tested.

The production of a structure in gypsum may nominally be divided into three major periods: the first is characterized by a thixotropic structure (from mixing to the start of setting), the second in the main by the formation of a primary crystallization structure (from the start to end of setting), and the third by strengthening in the structure (from the end of setting to completion of crystallization, as recorded from the maximum heat release).

For each of these periods we examined the strength in relation to the parameters of the magnetic fields (alternating and constant). The strength of the steady field was in the range from $1\cdot10^5$ to $4.4\cdot10^5$ A/m, while the frequency of the alternating field was in the range 30-380 Hz with a strength of 7960 A/m. These values were used in determining the optimum times for applying the fields and the optimum durations of action. The magnetic field is best applied as soon as possible after mixing, and even directly during the mixing. The optimum duration of action is τ_{du} = (0.25-0.5) τ_1, where τ_1 is the length of the first period above (Fig. 1). Either type of field applied in the first stage always increases the ultimate strength by comparison with standard specimens, and a magnetic field having the optimum parameters increases σ_{co} by 25-35%.

A magnetic field applied during the second period reduces the final strength, while one during the third period has no effect.

The subsequent experiments were designed to produce strong building materials by the combined action of several factors [3], the intention being to produce plaster specimens of strength in compression up to 1000 kgf/cm^2.

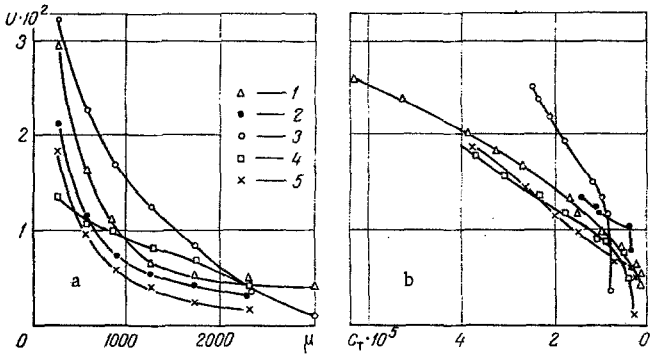

Fig. 3. Dependence of water content U (kg/kg) for: a) chemical potential μ (J/mole); b) isothermal mass capacity C_m (mole/J) for gypsum plaster: 1) standard hardening; 2,3) special treatment; 4) processed in a magnetic field with optimum parameters; 5) treated in a magnetic field.

We examined the porosity and thermodynamic parameters (mass transport) in order to elucidate the mode of action of external factors; the porosity determines major physicomechanical properties such as strength, long-term resistance, permeability to water and gases, thermal conductivity, and resistance to freezing. The size and structure of the pores control hydration, water binding, and the capacity for migration or infiltration of water.

The structural characteristics and the thermodynamic parameters were measured on the same specimens, which also provided information on the tendency to take up water and the effects from contact with other materials.

The porous structure may be determined for pores of radius 0.0015–0.05 μm along with measurement of the thermodynamic parameters for the mass transport by reference to water-vapor sorption isotherms with the equipment of [4].

We used standard specimens made in the standard way in accordance with GOST (All-Union State Standard) 125-70, which had a strength of 65 kgf/cm^2 in compression (No.1); in addition, there were specimens in series Nos.2 and 3, which were given special treatment (various combinations of several external factors [3]), which had σ_{co}, respectively, of 900–1000 and 700–800 kgf/cm^2; further, there were specimens in series Nos.4 and 5 which were treated with magnetic fields, with specimens of series No.4 having σ_{co} = 82 kgf/cm^2 being treated in a steady magnetic field having optimum parameters.

Before the experiments were begun, the gypsum was ground to a grain size of 0.25 mm and dried at 10^{-1} mm Hg for 336 h.

The sorption isotherms were determined at 303°K at relative pressures of 0.1–1 for 16 h; Fig. 2 shows that the maximum hygroscopic water content was higher for specimen No.1 by a factor of 4 than that for specimen No.2 and by a factor of 2 for specimens Nos.3 and 4.

The sorption isotherms were used to determine the binding energy (in the hygroscopic range, this is equal in magnitude to the chemical potential $\mu = RT \ln \varphi$ for mass transport) together with the isothermal specific mass capacity $C_m = (\partial U/\partial \mu)_T$ (Fig. 3), and the distribution of the pores by radius.

Figure 3 indicates that there are various forms of bond between the material and water, and it defines the transition from the adsorbed form to the capillary form. The binding energy falls considerably, while the isothermal specific mass capacity increases, at a water content of 0.45% for specimen No.1, as against 1.1 and 1.2% for specimens Nos.2 and 3, and 0.64 and 0.7% for specimens No.4 and 5. These ranges correspond to the transition from adsorption to capillary binding for these specimens.

It is clear that plaster made in the standard way has much of the water bound by capillary forces, whereas the special treatment causes much of the water to be in adsorbed form. The mean isothermal specific mass capacity (Fig. 3) is highest for the normal specimens and lowest for the specially treated ones.

The sorption results gave the pore-size distribution via the corrected model-free method [5].

The porous structure of gypsum (pore size range 0.01–22 μm) has been examined [6] by forcing in mercury at high and low pressures; the result is an integral curve, i.e., the pore volume as a function of equivalent radius (Fig. 4a).

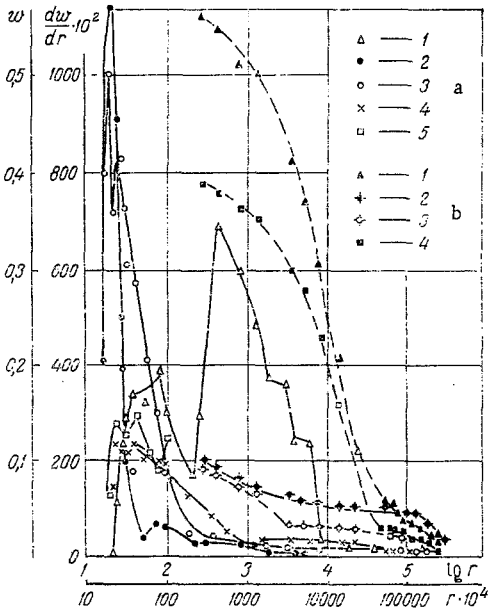

Fig. 4. Integral pore distributions (w in cm^3/g) (a) and differential distribution in radius $\partial w/\partial r$ ($cm^3/g \cdot \mu m$) (b) in relation to log r (r in μm): 1) standard hardening; 2, 3) special treatment; 4) processed in a magnetic field with optimum parameters; 5) treated in a magnetic field.

The total volume of the pores of radii from 22 to 0.01 μm for the standard specimen exceeds by a factor of 5 the same for specimens Nos. 2 and 3, and by a factor of 1.4 that for the specimen treated in magnetic fields. The integral curves may be differentiated graphically (fourth-difference method) to plot $\Delta w/\Delta r$ as a function of log r.

Figure 4b shows differential distributions for all the specimens between 0.0015 and 22 μm as derived from the sorption data and mercury measurements. The latter agree well with the former.

Specimen No. 2 had a sharp peak at r of about 0.0018 μm, and also a minor peak around 0.007 μm.

Specimen No. 3 had two peaks at about 0.0018 and 0.0023 μm; the latter is less sharp and extends up to 0.01 μm. Therefore, specimen No. 3 has mainly pores of radii between 0.0018 and 0.01 μm, with most of the pores in the range 0.0018-0.0025 μm.

The standard specimen had two peaks in the ranges 0.005-0.01 and 0.02-0.6 μm; small pores ($r < 0.0025$ μm) were absent in this specimen.

Specimen No. 4 (treated in an optimal magnetic field) had two peaks in the range 0.0025-0.01 μm; specimen No. 5 had a low broad peak in the region 0.0023-0.02 μm, and pores of radius 0.0025-0.02 μm predominate in these specimens.

The total volume of all pores up to 20 μm inclusive was 0.62 cm^3/g for the standard specimen, as against 0.144 for specimen No. 3 and 0.426 for specimen No. 5 (treated in a magnetic field).

Specimens Nos. 2 and 3 had not only lower pore volumes, but also mainly small pores (radii 0.0018-0.0023 μm). The standard specimen had a total pore volume five times that found in specimen No. 2 and 4.4 times that in specimen No. 3, while pores of radius less than 0.0025 μm were completely absent.

This all indicates that the strengths of specimens Nos. 2 and 3 should be much in excess of the strength of the standard specimen; in fact, the strengths in compression for those two specimens were 10-15 times σ_{co} for the standard one.

The plaster after magnetic-field treatment had a total pore volume reduced by a factor of 1.5 relative to the standard specimen, and the pores were mainly in the size range 0.0023-0.02 μm.

Therefore, the water-binding form and the specific mass capacity thus provide data in good agreement with those from the structural and strength characteristics.

These results on the structural and other features of high-strength plaster indicate that the latter can be used in facing components instead of costly granite or marble.

LITERATURE CITED

1. V. G. Kamenskii, G. S. Raptunovich, I. M. Lyashkevich, V. P. Samtsov, and L. N. Mankevich, in: Line-Ac Heat Treatment of Reinforced-Concrete Components and Constructions [in Russian], Minsk (1975), p.70.
2. G. S. Raptunovich, I. M. Lyashkevich, V. P. Samtsov, and I. L. Poleshchuk, in: Line-Ac Treatment of Reinforced-Concrete Components and Constructions [in Russian], Minsk (1975), p.165.
3. V. G. Kamenskii, I. M. Lyashkevich, G. S. Raptunovich, V. P. Samtsov, and A. A. Potapov, Positive Decision on Application No.2031819/29-33.
4. V. A. Karelina and E. A. Raskina, in: Heat Physics of Buildings [in Russian], Minsk (1973).
5. S. Brunauer, R. Sh. Mikhail, and E. E. Bodor, J. Colloid. Interface Sci., 24, 451 (1967).
6. T. G. Plachenov, The P-5 Mercury Porometer System [in Russian], Lensovet Polytekh. Inst., Moscow–Leningrad (1961).

OPTIMAL HEATING SURFACE IN A MULTISTAGE COUNTERCURRENT FLUIDIZED-BED HEAT EXCHANGER

A. K. Visloguzov

UDC 66.096.5-536.24

Equations are derived for calculating the intermediate temperatures of the heating medium such as to give the minimal total surface area in a multistage countercurrent heat exchanger having tubes immersed in a fluidized bed.

Heat exchangers having surfaces immersed in fluidized beds are increasingly being used in industry, on account of the properties of fluidized beds such as high heat-transfer coefficient, isothermal conditions in the bed, and absence of local overheating.

On the other hand, the isothermal condition is a disadvantage, since it restricts the maximum temperature of the cooling medium. The heat-balance equation for a one-stage exchanger is as follows (here and subsequently it is assumed that the heating medium passes within the tubes, while the cooler medium passes through the bed):

$$w(t_1 - t_2) = \theta_1 - \theta_2, \tag{1}$$

which goes with the condition for the temperature difference between the heating fluid and the cooling one:

$$t_2 \geqslant \theta_1, \tag{2}$$

which gives an expression for the temperature of the cooler fluid in a one-stage equipment; in the limiting case, for $t_2 = \theta_1$, the maximum temperature in the cooler medium is

$$\theta_{1\max} = \frac{wt_1 + \theta_2}{1 + w}. \tag{3}$$

One therefore usually employs a multistage system in order to raise the final temperature of the cooler medium.

The gas temperature falls in a single stage of a fluidized-bed heat exchanger, while the temperature of the bed remains constant, and therefore one cannot say one has countercurrent flow or direct flow in a single stage; however, in a multistage system it is possible to distinguish the two types.

In a direct-flow system, the two fluids enter the first stage and pass in series through all stages to emerge from stage n. In the countercurrent case, the two fluids enter at opposite ends of the chain and move in opposite directions.

Translated from Inzhenerno-Fizicheskii Zhurnal, Vol.31, No.1, pp.60-65, July, 1976. Original article submitted May 7, 1975.